

## Low-frequency switching in a transistor amplifier

T. L. Carroll

U.S. Naval Research Laboratory, Washington, D.C. 20375

(Received 9 December 2002; published 17 April 2003)

It is known from extensive work with the diode resonator that the nonlinear properties of a  $P$ - $N$  junction can lead to period doubling, chaos, and other complicated behaviors in a driven circuit. There has been very little work on what happens when more than one  $P$ - $N$  junction is present. In this work, the first step towards multiple  $P$ - $N$  junction circuits is taken by doing both experiments and simulations with a single-transistor amplifier using a bipolar transistor. Period doubling and chaos are seen when the amplifier is driven with signals between 100 kHz and 1 MHz, and they coincide with a very low frequency switching between different period doubled (or chaotic) wave forms. The switching frequencies are between 5 and 10 Hz. The switching behavior was confirmed in a simplified model of the transistor amplifier.

DOI: 10.1103/PhysRevE.67.046208

PACS number(s): 05.45.Jn, 84.30.-r

### I. INTRODUCTION

Because of electromagnetic interference (which may be unintentional or intentional) [1], many circuits designed for low-frequency operation may be subjected to radio frequency (rf) signals. At high frequencies, the inductance in the wiring of these circuits combined with capacitance in semiconductor  $P$ - $N$  junctions can cause resonances, exposing the circuit to larger rf voltages than anticipated by the circuit designer. The large voltages, combined with the nonlinear voltage-dependant capacitances of the  $P$ - $N$  junctions, can cause nonlinear effects such as period doubling, chaos, and others. The simplest example of this type of effect is the diode resonator [2–10], which has been extensively studied.

There has been very little study of semiconductor circuits containing more than one  $P$ - $N$  junction. Period doubling and chaos have been observed in a transistor amplifier circuit [11], and in a microwave amplifier [12], but there has been no analysis and only very simple modeling of these effects in circuits more complicated than the diode resonator. There have been several chaotic oscillator circuits based on transistors [13–15], but those were self-oscillatory circuits designed to be chaotic, while the present paper concerns a nonoscillatory circuit which is driven outside the range for which it was designed.

In this work, a single-transistor amplifier is studied experimentally and numerically. Not only are period doubling and chaos observed, but very low-frequency switching between different complex wave forms is also seen. The low-frequency behavior was seen both in the experiment and in a numerical model. This low-frequency behavior could complicate the use of the amplifier when electromagnetic interference was present.

### II. THE TRANSISTOR

The amplifier in the paper is based on a 2n929 transistor, a bipolar  $N$ - $P$ - $N$  transistor. Figure 1 is a simple block diagram of a transistor. The three terminals of the transistor are labeled base, collector, and emitter. In this  $N$ - $P$ - $N$  transistor, the base is a layer of  $P$ -type semiconductor material, while the collector and emitter are  $N$ -type, so that the transistor

looks like two back-to-back  $P$ - $N$  junctions. The transistor is not the same as two back-to-back diodes because most of the current flowing from the collector or emitter into the base continues flowing through the base into the emitter or collector.

The resistors labeled  $R_{NC}$  or  $R_{NE}$  represent the nonlinear resistances of the  $P$ - $N$  junctions making up the transistor. In the simplest model, the resistors conduct no current until the voltage across them reaches some threshold, at that point the nonlinear resistance conducts current. The arrows on the nonlinear resistors indicate the direction of easy current flow. The actual behavior is more complicated. The functioning of the nonlinear resistances in the transistor may be described by the Ebers-Moll equations [16]. For an  $N$ - $P$ - $N$  transistor, such as the 2n929 used in the experiments above, the equations are

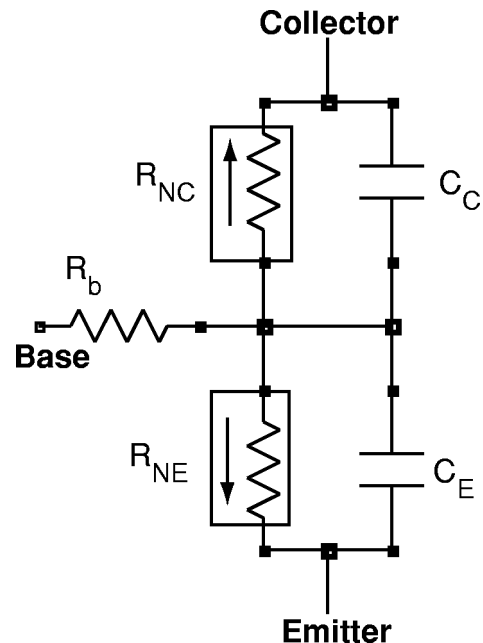


FIG. 1. Block diagram of an  $N$ - $P$ - $N$  transistor.  $R_b$  represents the base resistance of  $\approx 50 \Omega$ , while  $R_{NC}$  and  $R_{NE}$  represent the nonlinear resistances of the transistor.  $C_C$  and  $C_E$  represent the capacitances of the transistor.

$$I_C = I_0 [ - (e^{-qV_{CB}/kT} - 1) + \alpha (e^{qV_{BE}/kT} - 1) ], \quad (1a)$$

$$I_E = I_0 [ (e^{qV_{BE}/kT} - 1) - \alpha (e^{-qV_{CB}/kT} - 1) ], \quad (1b)$$

$$I_B = I_C - I_E, \quad (1c)$$

where  $I_C$  is the current flowing into the collector,  $I_B$  is the current flowing into the base, and  $I_E$  is the current flowing out of the emitter.  $V_{CB}$  is the collector-base voltage,  $V_{BE}$  is the base-emitter voltage,  $q$  is the charge of one electron,  $k$  is the Boltzman constant,  $T$  is the temperature in Kelvin, and  $\alpha$  is the fraction of current that flows from the collector, through the base, and into the emitter (or in the reverse direction). The fraction  $\alpha$  is typically just below 1.0: for the 2n929 transistor, it was measured as 0.995.

Each  $P$ - $N$  junction also stores some charge, so the charge storage is represented by a capacitor in parallel with the non-linear resistor. There are actually two types of charge storage in the  $P$ - $N$  junction [16], so  $C_C$  and  $C_E$  in Fig. 1 really stand for two capacitors in parallel. There is region at the actual junction between  $P$ - and  $N$ -type semiconductors that is depleted of charge, and this region acts like the dielectric in a parallel-plate capacitor. The charge stored in this capacitor leads to the junction capacitance  $C_J(V)$  (where  $V$  is the voltage across the  $P$ - $N$  junction) [17]

$$C_J(V) = \frac{C_J(0)}{[(V - V_b)^2 + b]^{n/2}} \left( 1 + \frac{n}{1-n} \frac{b}{[(V - V_b)^2 + b]} \right), \quad (2)$$

where  $V_b$  is the built-in voltage (approximately the turn on voltage) for the junction,  $V$  is the voltage across the junction, and  $b$  and  $n$  may be estimated by measuring junction capacitance as a function of  $V$  for  $V < V_b$ . Equation (2) is actually an approximation that is accurate only for  $V < V_b$ , but for  $V > V_b$ , the second type of capacitance described below dominates.

Outside of the depletion region, minority carriers diffuse into the bulk of the semiconductor, leading to the diffusion capacitance  $C_D(V)$

$$C_D(V) = C_D(0) e^{qV/kT}, \quad (3)$$

where  $q$  is the charge of one electron,  $k$  is the Boltzman constant, and  $T$  is the temperature in Kelvin.

In experiments with  $P$ - $N$  junctions (such as the diode resonator), the capacitance of the  $P$ - $N$  junction combines with stray inductance in the circuit wiring to form a series resonant circuit. Typical capacitances for  $P$ - $N$  junctions are of the order of  $10^{-12}$  F or less (1 pF), so these resonances occur at frequencies of 1 GHz or greater. Acquiring data and building circuits at such high frequencies is difficult, so in the experiment described here, an inductor was added to the circuit to increase the inductance of the wiring, therefore lowering the resonant frequency to a range between 200 kHz and 30 MHz. In many of the plots in this paper, the frequency axis is normalized by this resonant frequency.

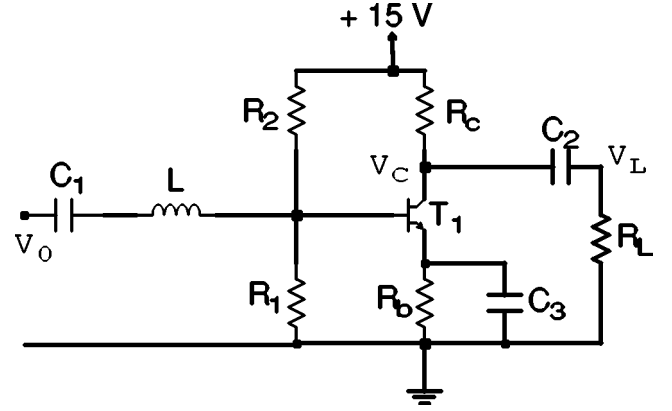


FIG. 2. Schematic of the amplifier circuit used in the experiments. The component values are  $R_1 = 40\,420\ \Omega$ ,  $R_2 = 204\,545\ \Omega$ ,  $R_C = 15\,000\ \Omega$ ,  $R_E = 3750\ \Omega$ ,  $R_L = 1\ M\Omega$ ,  $C_1 = C_2 = 25\ \mu\text{F}$ ,  $C_3 = 330\ \mu\text{F}$ ,  $L = 2200\ \mu\text{H}$ , and the transistor  $T_1$  is of type 2n929. The driving voltage is applied at the location marked  $V_0$  and the output voltage is measured at  $V_L$ .

### III. THE AMPLIFIER

Figure 2 is a schematic of the common-emitter amplifier used in the experiments. The transistor  $T_1$  is a 2n929 bipolar transistor. The inductor  $L$  has been added to the amplifier circuit to increase the inductance of the wiring so that the circuit behavior may be studied at lower frequencies. The output from the amplifier is the voltage  $V_L$  measured across the load resistor  $R_L$ . The values of the circuit components are given in the figure caption. Trim pots were used to create resistances that did not match standard resistance values.

The circuit was driven with a constant amplitude sine wave  $V_0$  generated by a digital function generator. In order to further isolate the signal generator from the circuit, the signal  $V_0$  was first passed through a broadband preamplifier which acted as a buffer. To lessen the effect of the detection electronics on the amplifier circuit, a  $100\ \text{k}\Omega$  resistor was placed between the location where  $V_L$  was measured and the detector.

### IV. EXPERIMENT

As the frequency and amplitude of the driving signal  $V_0$  were varied, period doubling and chaos were among the dynamical effects observed. Period doubling and chaos have been seen in other amplifier circuits [11,12] and in the diode resonator, so their presence was not surprising. What was surprising is that the dc level of  $V_L$  fluctuated slowly but periodically, oscillating at frequencies between 5 and 10 Hz. After passing through a  $100\ \text{k}\Omega$  resistor,  $V_L$  was low-pass filtered through an amplifier which filtered out signals above 1000 Hz, and the filtered  $V_L$  signal was digitized. Figure 3 is a time series of the low-pass filtered output, which shows regular switching (the inductor  $L$  was set to  $2200\ \mu\text{H}$ ). Figure 4 shows the beginning and end of one of these switching events, with no low-pass filtering.

The origin of this switching could be seen by digitizing the voltage  $V_C$ , which was the voltage at the collector of the transistor. An isolating probe was used to isolate the transi-

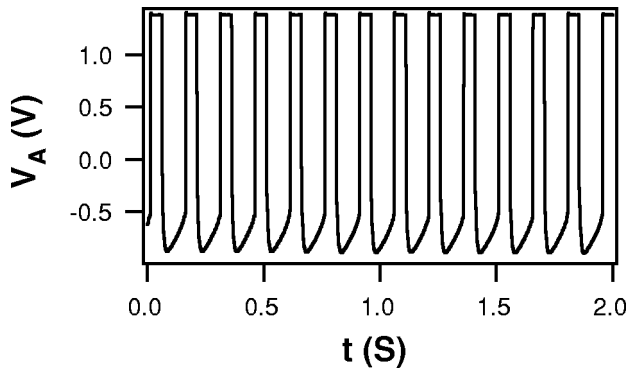


FIG. 3. Low-pass filtered signal  $V_L$  when low-frequency switching is present. The low-pass filter break frequency was 1 kHz.

tor circuit from the digital oscilloscope used to detect  $V_C$ . Two distinct states with different dc levels were observed for  $V_C$ . Figure 5(a) shows a plot of  $V_C$  vs  $V_0$  for the state corresponding to the higher dc level, while 5(b) is the state with the lower dc level. A slow but periodic switching between these two states was the cause of the low-frequency switching seen in the amplifier output.

The frequency of this slow switching varied depending on the value of  $V_0$ . Figure 6 is a plot of switching frequency as a function of the frequency and amplitude of  $V_0$ , with black being the highest frequency and white corresponding to no switching. The frequency axis  $f_n$  is normalized by the resonant frequency of the series resonant circuit consisting of the inductor and the transistor. The base-emitter junction of the transistor acts as the capacitor in the series resonant circuit. The base-emitter capacitance, which varied as a function of bias voltage, was measured in the laboratory for the 2n929

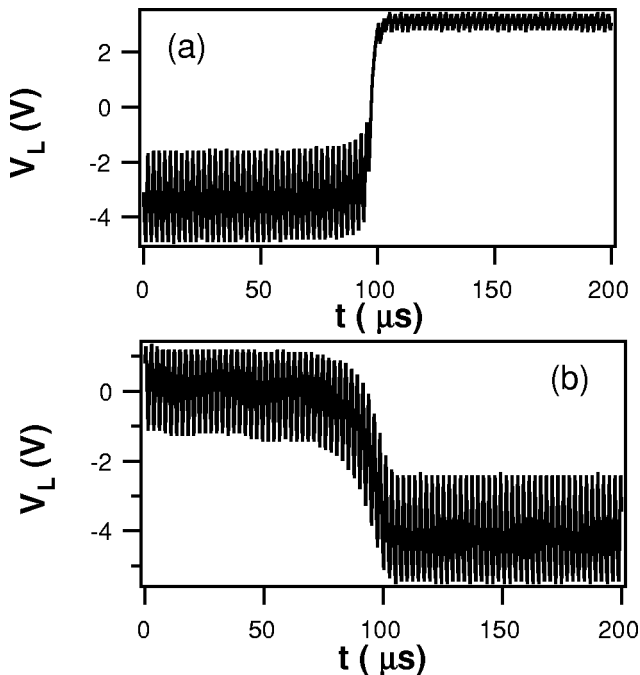


FIG. 4. (a) Unfiltered  $V_L$  signal at the start of a switching event. (b) Unfiltered  $V_L$  at the end of a different switching event. The time scale of a complete switching event was of the order of 0.1 s.

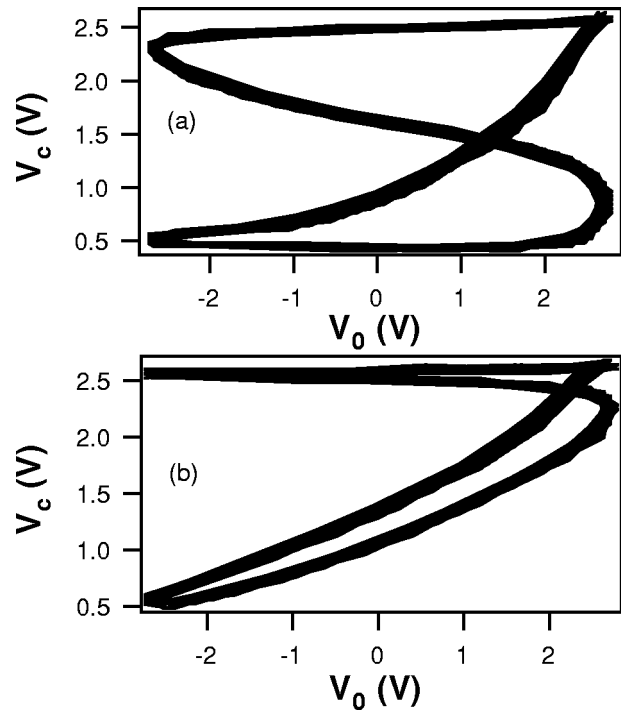


FIG. 5. Phase space plots of  $V_C$ , the voltage at the collector, vs the driving voltage  $V_0$  during the two different parts of a switching event. The two  $V_C$  wave forms have different dc components, leading to the large dc swings seen in Fig. 3.

transistor, and the capacitance at zero bias,  $C(0)=24$  pF, was used to calculate the resonant frequency of the series LCR circuit. A frequency of  $f_n=1$  corresponds to the resonant frequency of this circuit, which for  $L=2200$   $\mu$ H was  $\approx 693$  kHz.

The switching frequency is quite sensitive to the param-

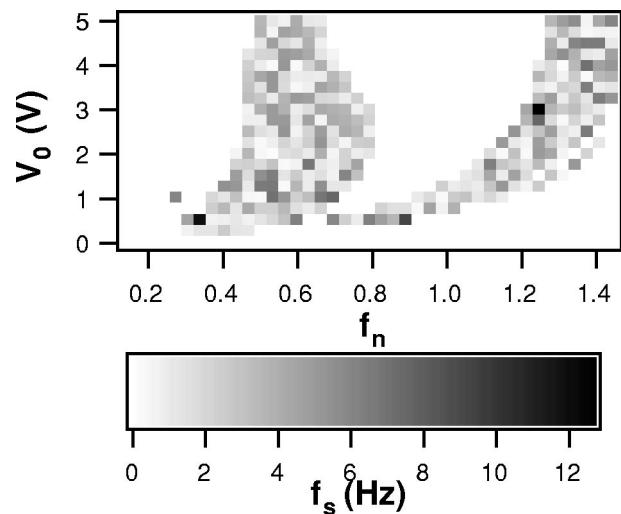


FIG. 6. Frequency of the slow switching for different amplitudes and frequencies of the driving signal, where black is the highest value and white corresponds to zero.  $f_n$  is the driving frequency normalized by the resonant frequency of the inductor-transistor series resonant circuit. The lower graph gives the frequency scale for the upper graph, where  $f_s$  is the switching frequency.

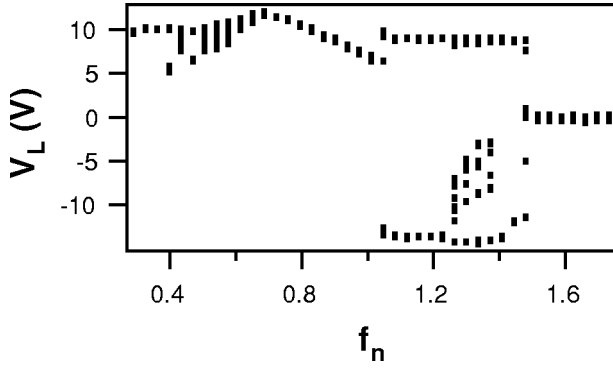


FIG. 7. Bifurcation plot of  $V_L$  from the transistor amplifier experiment strobed when the driving signal  $V_0$  crosses zero in the negative direction.  $f_n$  is the driving frequency normalized by the resonant frequency of the inductor-transistor series resonant circuit. The amplitude of the driving signal was 5 V. The regions where period two or higher behavior was seen in the bifurcation plot coincide with the regions where slow switching was seen.

eters of the driving voltage, and there is a large region near the resonant frequency where no switching is seen. The bifurcation diagram in Fig. 7 shows why there is no switching in this region. The bifurcation diagram was created by plotting the value of  $V_C$  when the driving signal  $V_0$  crossed zero in the negative direction. The amplitude of  $V_0$  for the bifurcation diagram was 5 V. The bifurcation diagram shows that low-frequency switching exists only when attractors higher than period one exist. There is only one period one state, but there are at least two distinct types of wave form for states with periods higher than one.

There was a lower driving frequency limit below which switching was not seen. Switching was observed for a resonant frequency of 459 kHz ( $L=5000 \mu\text{H}$ ), but not for a resonant frequency of 383 kHz ( $L=7200 \mu\text{H}$ ), although period doubling was seen for this resonant frequency. Low-frequency switching was seen when the resonant frequency of the inductor-transistor combination was 10.2 MHz ( $L=10 \mu\text{H}$ ), but neither period doubling or low-frequency switching was seen for a resonant frequency of 32 MHz ( $L=1 \mu\text{H}$ ). It has been shown in the diode resonator that period doubling for higher driving frequencies can be suppressed by the stray capacitance of the breadboard on which the circuit is assembled [2], so it is possible that low-frequency switching could also exist at higher driving frequencies.

## V. NUMERICAL SIMULATIONS

Numerical simulations are useful to confirm that the dynamical effects seen are indeed part of the transistor amplifier, and not caused by some other effect, such as an interaction with the driving signal source or the detection electronics. The simulations can also reveal if the model used for the transistor is adequate to produce the effects seen in the experiment.

The transistor may be described by Eqs. (1)–(3), but the resulting model is difficult to work with. The exponential terms in Eqs. (1) and (3) make the resulting equations of

motion stiff, requiring the use of a stiff numerical integration routine. Stiff routines are slower than integrators that are not stiff [18], and integration speed is a matter of concern in this problem. The amplifier circuit was driven at frequencies of the order of 1 MHz, while the switching events occurred at frequencies of a few Hertz, so very long integration times will be necessary to model the switching. In order to make the simulations more practical, a simpler piecewise linear model for the transistor was substituted. A disadvantage of changing to the piecewise linear model is that there is no longer a direct correspondence between the model parameters and the measurable physical parameters of the transistor.

The combined capacitances for the transistor were replaced with a single piecewise linear model. A similar model was used by Tanaka [8]. The capacitance model used here is

$$C_n(V,s) = \begin{cases} C_0, & |V| \leq V_{b1} \\ s(m_n V + b_n), & |V| > V_{b1} \end{cases}, \quad (4a)$$

$$b_n = s(C_0 - m_n V_{b1}), \quad (4b)$$

where  $V$  is the voltage across the junction,  $s$  is  $-1$  for the collector-base junction and  $+1$  for the base-emitter junction (the signs would be reversed for a  $P-N-P$  transistor),  $V_{b1}$  is 0.5 V, the zero bias capacitance  $C_0$  is 24 pF, and the slope  $m_d = 500 \text{ pF/V}$  (the value of the slope was arbitrary).

The nonlinear current equations [Eq. (1)] were also replaced with

$$I_C = I_0 [g_n(V_{CB}, -1) + \alpha g_n(V_{BE}, 1)], \quad (5a)$$

$$I_E = I_0 [g_n(V_{BE}, 1) + \alpha g_n(V_{CB}, -1)], \quad (5b)$$

$$I_B = I_C - I_E, \quad (5c)$$

$$g_n(V,s) = \begin{cases} 0, & |V| \leq V_{b2} \\ m_1 V + b_1, & |sV| > V_{b2} \end{cases}, \quad (5d)$$

$$b_1 = s m_1 V_{b2}, \quad (5e)$$

where the slope  $m_1 = 10^{-4} \text{ A/V}$ , and the turn-on voltage  $V_{b2}$  was 0.6 V. The break point voltage in the capacitance function of Eq. (4) ( $V_{b1}$ ) was slightly less than the turn-on voltage  $V_{b2}$  because the capacitance value starts to rise before the transistor turns on.

The slope constant  $m_1$  in Eq. (5) was set by simulating the characteristic curves for the transistor, where the collector current  $I_C$  is plotted as a function of the collector-emitter voltage  $V_{CE}$  for different levels of the base current  $I_b$  [19]. Figure 8 shows a characteristic curve plot for the 2n929 transistor (measured experimentally), where the base current values for the curves were  $0.5 \mu\text{A}$ ,  $1.7 \mu\text{A}$ ,  $2.9 \mu\text{A}$ ,  $4.1 \mu\text{A}$ , and  $5.3 \mu\text{A}$ . Figure 9 shows the characteristic curves from the piecewise linear simulation, with base current values of  $0.19 \mu\text{A}$ ,  $0.67 \mu\text{A}$ ,  $1.1 \mu\text{A}$ ,  $1.6 \mu\text{A}$ , and  $2.1 \mu\text{A}$ . These plots are a standard method for characterizing a transistor. The simulated curves were compared with actual curves, and

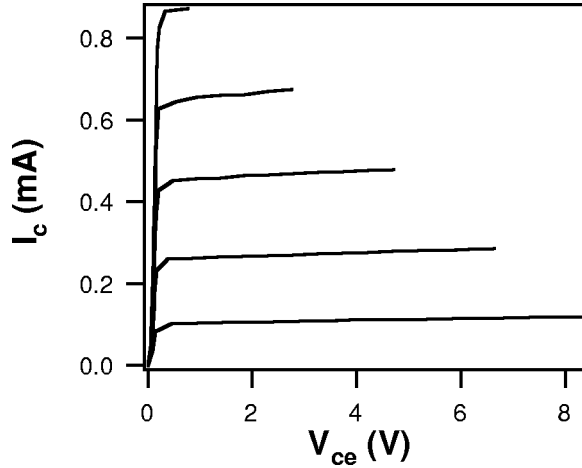


FIG. 8. Characteristic curves of the collector current  $I_C$  vs the collector-emitter voltage  $V_{CE}$  at different base currents for the 2n929 bipolar transistor used in the circuit of Fig. 1. The base currents for these curves (starting at the bottom) were  $0.5 \mu\text{A}$ ,  $1.7 \mu\text{A}$ ,  $2.9 \mu\text{A}$ ,  $4.1 \mu\text{A}$ , and  $5.3 \mu\text{A}$ .

$m_1$  was chosen to make the simulations roughly match the experimental curves. The full equations of motion for the transistor amplifier were

$$\frac{dx_1}{dt} = - \left( \frac{J_1 + I_C R_c R_l}{R_c R_l C_n(x_1, -1)} \right), \quad (6a)$$

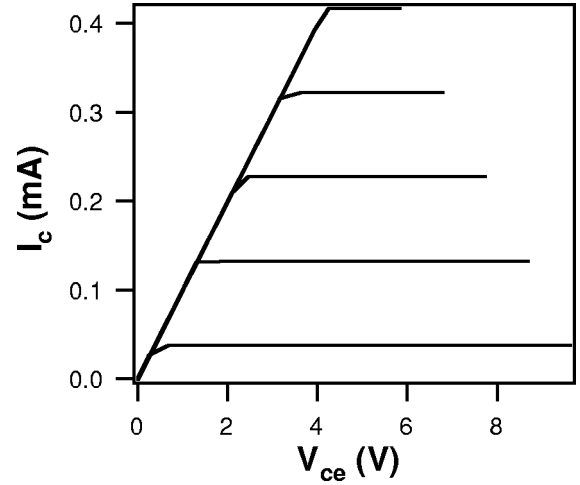


FIG. 9. Characteristic curves of the collector current  $I_C$  vs the collector-emitter voltage  $V_{CE}$  at different base currents for the piecewise linear model of a transistor amplifier. The base currents for these curves (starting at the bottom) were  $0.19 \mu\text{A}$ ,  $0.67 \mu\text{A}$ ,  $1.1 \mu\text{A}$ ,  $1.6 \mu\text{A}$ , and  $2.1 \mu\text{A}$ .

$$\frac{dx_2}{dt} = - \left( \frac{J_4 R_1 + J_5 R_2 + I_e R_c R_l R_A}{R_c R_l R_A C_n(x_2, 1)} \right), \quad (6b)$$

$$\frac{dx_3}{dt} = \frac{- \left( \frac{R_1 (R_b V_a + R_2 R_b x_3 + R_2 x_4)}{R_1 R_2 + R_1 R_b + R_2 R_b} \right) + x_5}{L}, \quad (6c)$$

$$\frac{dx_4}{dt} = \frac{I_e + \frac{x_2}{R_e} - \frac{x_4}{R_e} - \frac{(J_4 R_1 + J_5 R_2 + I_e R_c R_l R_A) [C_6 + C_n(x_2, 1)]}{R_c R_l R_A C_n(x_2, 1)}}{C_6}, \quad (6d)$$

$$\frac{dx_5}{dt} = \frac{dV_0}{dt} - \frac{x_3}{C_1}, \quad (6e)$$

$$J_4 = [J_2 R_2 + J_1 R_b + R_c R_l (-V_a + x_4)], \quad (6k)$$

$$J_5 = (J_1 R_b + R_c R_l x_4). \quad (6l)$$

$$\frac{dx_6}{dt} = \frac{I_e R_e + x_2 - x_4}{C_6 R_e} - \frac{x_6}{C_l R_l} - \frac{J_1 + I_C R_c R_l}{R_c R_l C_n(x_1, -1)} - \frac{(J_4 R_1 + J_5 R_2 + I_e R_c R_l R_A) [C_6 + C_n(x_2, 1)]}{C_6 R_c R_l R_A C_n(x_2, 1)}, \quad (6f)$$

$$R_A = [R_2 R_b + R_1 (R_2 + R_b)], \quad (6g)$$

$$J_1 = [R_l (-V_a + x_1 + x_4) + R_c x_6], \quad (6h)$$

$$J_2 = [R_l (V_1 - R_c x_3) + R_c x_6] \quad (6i)$$

$$J_3 = [J_2 + J_1 R_b + R_c R_l (-V_a + x_4)], \quad (6j)$$

$V_a$  is the power supply voltage of +15 V. The variable  $x_1$  corresponds to the collector-base voltage,  $x_2$  corresponds to the base-emitter voltage,  $x_3$  is the current through the inductor  $L$ ,  $x_4$  is the voltage at the base of the transistor,  $x_6$  is the voltage at the junction of the input capacitor  $C_1$  and the inductor  $L$ , and  $x_6$  is the voltage across the load resistor  $R_L$ . Voltages other than  $x_1$  and  $x_2$  were referenced to ground.  $R_b$  is added to the model to simulate the base resistance of  $\approx 50 \Omega$ , and the inductor  $L$  was set to  $2000 \mu\text{H}$ , while all other component values are the same as in the circuit. The terms  $R_A$  and  $J_1$  through  $J_5$  do not have any particular units, but are added to make it possible to write the equations on one page.

The large separation in time scales between the driving frequency and the response frequency of the transistor am-

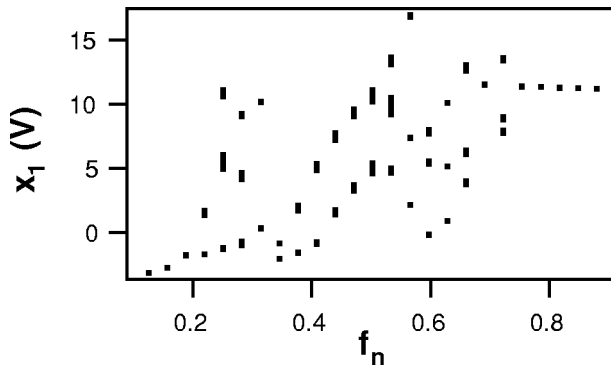


FIG. 10. Bifurcation plot from the model of Eq. (6), with a driving amplitude of 15 V.  $f_n$  is the driving frequency normalized by the resonant frequency of the inductor-transistor series resonant circuit. The  $x_1$  signal was strobed on the positive-going zero crossing of the driving signal.

plifier made it impractical to do extensive parameter variation studies, so the model was used only to verify that the low-frequency switching was indeed possible in the transistor amplifier circuit by itself, and not caused by some other artifact of the experiment.

In the experiment, it was observed that varying the values of the capacitors  $C_1$ ,  $C_2$ , and  $C_3$  by a factor of 10 neither affect the driving frequencies or amplitudes at which low-frequency switching was seen, nor was the distribution of switching frequencies affected. Since the results of the experiment were not very sensitive to the values of these capacitors, for the simulation they were all set to 1  $\mu\text{F}$  in order to reduce the length of the initial transient in the simulations.

The simulations of Eq. (6) used a fourth-order Runge-Kutta integration routine [18] with a stepsize of  $10^{-8}$  s. Each simulation was first run for 20 000 000 steps to eliminate the long initial transient. Figure 10 is a bifurcation plot from Eq. (6), where  $f_n$  is the driving frequency divided by the inductor-transistor resonant frequency of 795 kHz and  $x_1$  is the value of  $x_1$  when the driving signal crosses zero in the positive direction. The driving amplitude for Fig. 10 was 15 V. Signal amplitudes in the piecewise linear model do not correspond directly to signal amplitudes in the actual amplifier. The bifurcation plot does show regions of complex behavior, but unlike the experiment, all of this behavior occurs only for frequencies below the resonant frequency. Figure 11 shows a time series of the value of  $x_1$  at the positive-going zero crossings of the driving signal, for a driving frequency of 500 kHz ( $f_n=0.63$ ). Low-frequency switching between two different types of behavior is clearly seen. The switching frequency is 115 Hz. Figure 12 shows Poincaré sections from the two different types of oscillation. Figure 12(a) is a Poincaré section of  $x_2$  vs  $x_1$  for the larger oscillation, while (b) is a Poincaré section for the smaller oscillation. As in the experiment, different wave forms are present during the two different types of oscillation.

## VI. CONCLUSIONS

This paper has shown that driving a transistor amplifier with a high-frequency signal can cause very low-frequency

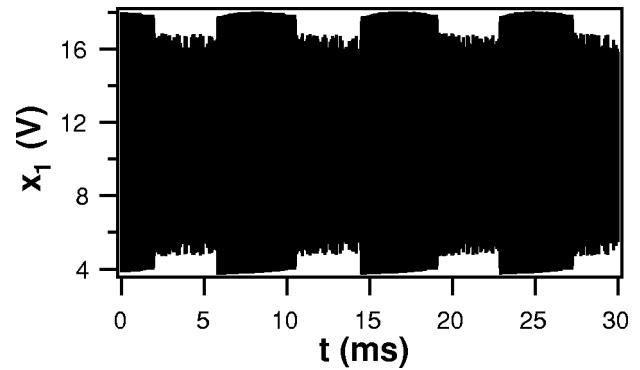


FIG. 11. Time series of the strobed  $x_1$  signal from the model of Eq. (6), when the driving amplitude was 15 V and the driving frequency was 500 kHz ( $f_n=0.63$ ). The frequency of the large switching events is 115 Hz.

switching. The low-frequency switching was seen in an experiment, and its existence was confirmed in a simple piecewise linear model of the transistor amplifier.

No such switching has been reported in the well-studied diode resonator circuit, which has only a single  $P-N$  junction, so it is almost certain that the double  $P-N$  junction in the transistor is responsible for the switching. This switching was not observed in my laboratory in a back-to-back pair of diodes, but because of the narrow base layer of the transistor, it is not the same as a simple pair of diodes.

Low-frequency switching was seen in other types of tran-

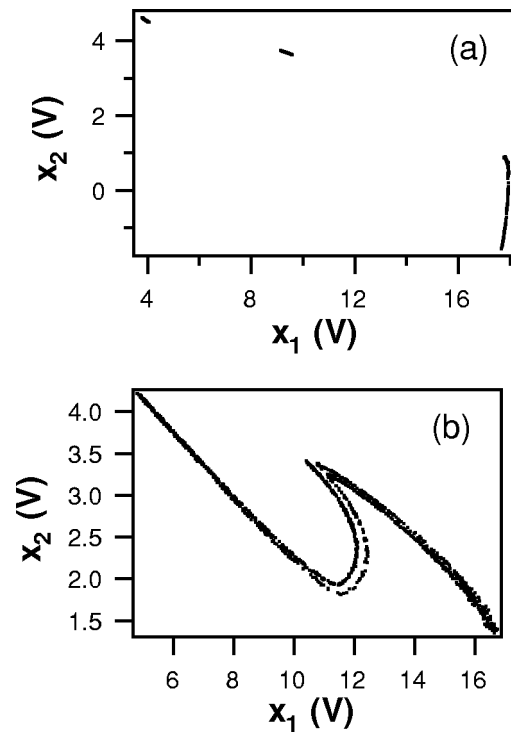


FIG. 12. Poincaré sections of two signals from the model of Eq. (6) (strobed at the positive-going zero crossing of the drive signal) for a drive amplitude of 15 V and frequency of 500 kHz. (a) is for the larger oscillation in Fig. 11, while (b) is for the smaller oscillation.

sistors besides the one reported here, including a metal-oxide-semiconductor field-effect transistor power transistor.

This paper does not address the cause of the low-frequency switching. The large frequency difference between

the driving signal and the switching means that specialized mathematical techniques for analyzing fast-slow systems must be employed. It is anticipated that further analysis will be undertaken in the future.

- 
- [1] V.I. Ponomarenko, M.D. Prokhorov, and Y.P. Seleznev, in *IEEE-Russia Conference on High Power Microwave Electronics: Measurements, Identification, Applications*, 1999, edited by A. Vostrikov (IEEE, Novosibirsk, Russia, 1999).
- [2] T.L. Carroll and L.M. Pecora, *Phys. Rev. E* **66**, 046219 (2002).
- [3] E.R. Hunt and R.W. Rollins, *Phys. Rev. A* **29**, 1000 (1984).
- [4] C.H. Kim, C.H. Cho, C.S. Lee, J.H. Yim, J. Kim, and Y. Kim, *Phys. Rev. A* **38**, 1645 (1988).
- [5] P.S. Lindsay, *Phys. Rev. Lett.* **47**, 1349 (1981).
- [6] Z. Su, R.W. Rollins, and E.R. Hunt, *Phys. Rev. A* **40**, 2698 (1989).
- [7] N. Takeuchi, T. Nagai, and T. Matsumoto, *Electron. Commun. Jpn.* **84**, 91 (2001).
- [8] S. Tanaka, S. Higuchi, and T. Matsumoto, *Phys. Rev. E* **54**, 6014 (1996).
- [9] J. Testa, J. Perez, and C. Jeffries, *Phys. Rev. Lett.* **48**, 714 (1982).
- [10] R.M.D. de Morales and S. Anlage (unpublished).
- [11] D.J. Jeffries, G.G. Johnstone, and J.H.B. Deane, *Int. J. Electron.* **71**, 661 (1991).
- [12] P. Perry, P. O'Halloran, and T.J. Brazil, in *Proceedings of the 3rd International Specialist Workshop on Nonlinear Dynamics of Electronic Systems* edited by M.P. Kennedy (IEEE, Dublin, Ireland, 1996).
- [13] M.P. Kennedy, *IEEE Trans. Circuits Syst., I: Fundam. Theory Appl.* **41**, 771 (1994).
- [14] A. Tamasevicius, G. Mykolaitis, S. Bumeliene, A. Cenys, A.N. Anagnostopoulos, and E. Lindberg, *Electron. Lett.* **37**, 549 (2001).
- [15] N.F. Rulkov and A.R. Volkovskii, *IEEE Trans. Circuits Syst., I: Fundam. Theory Appl.* **48**, 673 (2001).
- [16] M.J. Cooke, *Semiconductor Devices* (Prentice-Hall, Englewood Cliffs, 1990).
- [17] H.C. Poon and H.K. Gummel, *Proc. IEEE* **57**, 2181 (1969).
- [18] W.H. Press, B.P. Flannery, S.A. Teukolsky, and W.T. Vetterling, *Numerical Recipes* (Cambridge University Press, New York, 1990).
- [19] U. Tietze and C. Shenk, *Electronic Circuits* (Springer, Berlin, 1991).